Real-time vision-based control of industrial manipulators for layer-width setting in concrete 3D printing applications

E. Shojaei Barjuei, E. Courteille, D. Rangeard, F. Marie, A. Perrot

Advances in Industrial and Manufacturing Engineering 5 (2022) 100094

Contents lists available at ScienceDirect

Advances in Industrial and Manufacturing Engineering

journal homepage: www.elsevier.com/locate/aime

Real-time vision-based control of industrial manipulators for layer-width setting in concrete 3D printing applications

E. Shojaei Barjuei [a,*], E. Courteille [a], D. Rangeard [a], F. Marie [a], A. Perrot [b]

[a] University of Rennes, INSA Rennes, LGCGM, 35043 Rennes Cedex, France
[b] Univ. Bretagne-Sud, UMR CNRS 6027, IRDL, F-56100, Lorient, France

ARTICLE INFO

MSC:
00-01
99-00

Keywords:
Robotic concrete 3D printing
Extrusion-based additive manufacturing
Real-time vision-based control
Edge detection algorithm
Layer-width setting

ABSTRACT

In this paper, to have control over geometry specifications of rectangular bar-shaped layers in a robotic concrete 3D printing process, a real-time vision-based control framework is developed and proposed. The proposed control system is able to set the layer-width by automatically adjusting the velocity of an industrial manipulator during the 3D printing process of concrete based materials relying on a vision system feedback. Initially, details related to the control system, vision and processing units, and robotic platform are discussed. In continue, technical descriptions related to the printhead design, conversion process from a digital 3D drawing model to numerical motion control commands of an industrial manipulator and building material used in this work are reported. The reliability and responsiveness of the developed system is then evaluated through experimental tests by printing several single bar-shaped layers with different wideness by means of an unique printhead geometry and also by printing two layers with the same dimension centrally above another. Overall, the high accuracy and responsiveness of the developed system demonstrate a great potential for real-time vision-based control of industrial manipulators for layer-width setting in concrete 3D printing applications.

1. Introduction

Over the last few decades, the role of additive manufacturing, commonly known as 3D printing, in the construction industry has become gradually important (Armstrong and Alleyne, 2021). 3D printing is an automated process for fabricating 3D objects from computer-aided design (CAD) models. In this process, 3D models are subdivided into several layers which are subjected to be deposited in order to construct the designed objects (Valizadeh and Wolff, 2022). Even though applications and developments of 3D printing technologies can be found in different sectors, such as military, aerospace and bio-medicine (Chan et al., 2018; Bozkurt and Karayel, 2021), it has currently achieved significant attentions in manufacturing methods for cement-based constructions purposes (Sotorrío Ortega et al., 2020; Perrot et al., 2020; Zhang et al., 2021; Mazhoud et al., 2019).

Among the developed and presented methods and techniques for construction 3D printers, the extrusion-based additive manufacturing approaches have been the most investigated and studied (Perrot et al., 2018). In this technique, the cement-based material is dispensed precisely at predefined locations by means of a printhead (extruder). Accordingly, the printhead moves in a 3D space based on a predetermined path to build up a predesigned object in a layer-by-layer way (Hoffmann et al., 2020). It is worth to mention that the success of this process highly depends on the material structural build-up rate and the construction rate (Perrot et al., 2016b). Nematollahi et al. in Nematollahi et al. (2017) report some remarkable benefits of using extrusion-based additive manufacturing methods in respect of reducing the construction cost and time, reducing the injury rates and increasing architectural freedom. Several types of construction 3D printers such as Cartesian robots (Costanzi et al., 2018), robotic arms (manipulators) (Lim et al., 2020), cable driven parallel robots (Tho and Thinh, 2021) and Delta robots (Asprone et al., 2018) are currently in use and various objects (Hoffmann et al., 2020) have been produced by these robotic platforms. In a concrete 3D printing process, printing speed, printhead shut-off system, stand-off distance (SOD) and temperature are parameters which are needed to be controlled and predefined as they affect the shape, quality and behavior of printed concrete objects (Panda et al., 2019; Rushing et al., 2019). Whereas material extrusion-based additive manufacturing approaches can be subdivided into different categories (Zhang and Liou, 2021), the focus of this work is on the extrusion of a very stiff material (also known as infinite brick strategy (Mechtcherine et al., 2020)). Using this deposit strategy offers the possibility of obtaining smooth surface without any layering or barreling effects that can be found with other common strategies like controlled pressing of layers. The visual aspect of the printed

* Corresponding author.
E-mail address: erfan.shojaei-barjuei@insa-rennes.fr (E. Shojaei Barjuei).

https://doi.org/10.1016/j.aime.2022.100094
Received 14 April 2022; Received in revised form 18 June 2022; Accepted 21 July 2022
Available online 26 July 2022

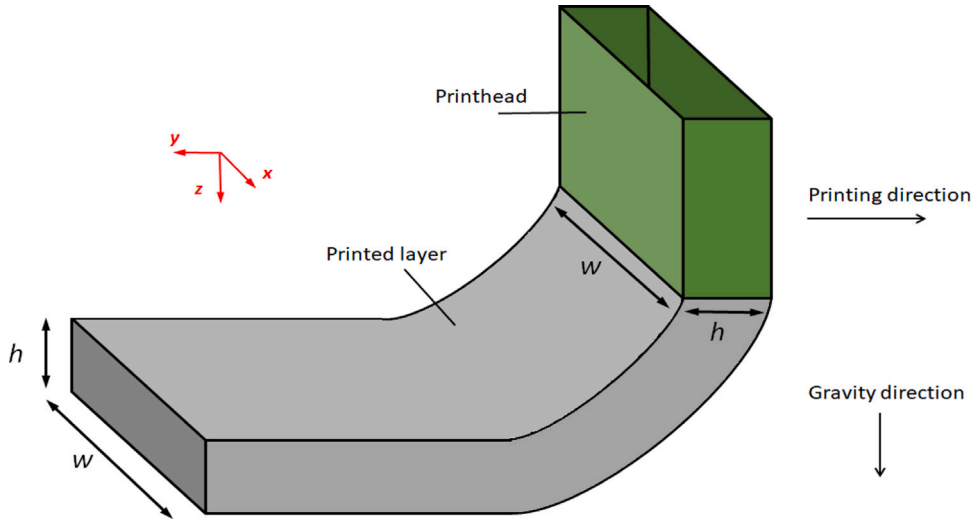

Fig. 1. Schematic drawing of extrusion of a very stiff material (infinite brick strategy) which creates layers with individual height h and width w.

structure is another important parameter that has forced researchers to find solutions such as troweling, rendering (Khoshnevis, 2004; Buswell et al., 2018; Bard et al., 2018) or methods based on the infinite brick strategy (Wolfs et al., 2021). A schematic drawing of an infinite brick strategy is depicted in Fig. 1. In this method, the shape of the printed object is strongly affected by the shape and outside diameter of the printhead nozzle because of the viscoelastic behavior of the fresh concrete (building material) (Wangler et al., 2016) and the cross-section of printed layer and printhead nozzle are equal in the ideal case. While circular nozzles make the 3D printing process simple as the nozzle is subjected to move along a predefined trajectory, employing rectangular nozzles is a challenging issue since it requires specific motion controlling techniques due to bulging corners which are mainly caused by material over-extrusion along indirect paths (Comminal et al., 2019; Carneau et al., 2020). This challenge becomes even more complex if the shape of the object geometry is not uniform over the entire of the layer path (Lao et al., 2018).

Apart from the extruder design, another fundamental factor that can effect the geometry quality of the printed object in the infinite brick strategy is the deposition speed of building material (Comminal et al., 2020). That is, if the printhead velocity is not perfectly synchronized with the extrusion flow rate, the final printed structure will not be neither continuous nor coherent (Nerella et al., 2019; Cheng and Jafari, 2008). Another challenging issue, caused by poor synchronization between the extrusion system and printhead velocity, is the extrusion width adjustment (Yan et al., 2022; Roussel, 2018). Theoretically, the extrusion width adjustment, or layer-width setting, is how width the nozzle extrudes a building material for each layer during a 3D printing process (Hsiang Loh et al., 2020). According to the works reported in Labonnote et al. (2016), Khan et al. (2020) and Carloni et al. (2021), an efficient layer-width setting can improve the accuracy and quality of 3D printed objects, strengthen the final structure and enhance the adhesion of the first (base) layer.

With the aim of ensuring geometrical specifications of the 3D printed objects, some authors have suggested and proposed approaches based on controlling the extrusion flow rate during the printing operations (Albar et al., 2020; Park et al., 2017; Jo et al., 2020; Yuan et al., 2022). However, these studies cannot be considered as conclusive solutions in applications where a building material must flow continuously through pipes or tubes to a printhead and finally extruded in layers. In fact, the challenging problem with these methods is the time that the pump takes to deliver a specific amount of building materials to the printhead (timed dosing) which makes the control operation very complicated. In a similar way, Kazemian et al. in Kazemian et al. (2019) have proposed a vision-based control strategy to regulate the extrusion flow rate based on geometry specifications of concrete 3D printed layers through a feedback from a vision system. Apart from a time delay in the control system due to a high nonlinear extrusion dynamics (Reinold et al., 2022) which limits the applications of feedback control approaches (Barjuei and Gasparetto, 2015), the non real-time nature of a such method degrades its performance in terms of under-extrusion and over-extrusion of the building material during the printing process. Remarkably, some other authors have proposed to use a feedback control by regulating extrusion velocity and/or force applied to the extruder (Zhao et al., 2010; Deuser et al., 2013; Greeff and Schilling, 2017). Although these methods can improve the deposition accuracy of steady-state extrusion and be enough robust against disturbances, they do not perform an accurate deposition during transients in material extrusion by changing the extrusion rate. This is mainly due to the fact that these techniques indirectly infer extrusion rate from extruder velocity and/or force. Using model-based control schemes has also been presented and proposed in some studies (Wu et al., 2021; Zomorodi and Landers, 2016; Lu et al., 2014) to create a synchronization framework among the extrusion flow rate and extruder motion velocity in order to mitigate deposition errors. In spite of significant reduction error in layer deposition under certain conditions, the key problem with such approaches is that principally the efficiency of a model-based control approach depends on a reliable and accurate dynamic model built into the controller structure (Barjuei et al., 2016). In additive manufacturing operations where process dynamics and parameters vary (Ducoulombier et al., 2021; Lu et al., 2019; Paolini et al., 2019), the dynamic model built into the controller hardly matches the system dynamics during printing operations so the controller performance degrades.

As discussed above, a new approach is therefore needed for improving the geometry quality of 3D printed layers in terms of the extrusion width, over- and under-extrusion. On this basis, the main objective of this study is to develop and propose a novel real-time vision-based control approach to create highly accurate rectangular bar-shaped layers in robotic concrete 3D printing applications. In contrast to studies in which the extrusion flow rate is the process to be controlled, in this work, the 3D printing process adjustment is made by regulating the printing speed and keeping the extrusion flow rate constant. In particular, the proposed solution: (1) leads to a highly accurate and robust control framework with a high-bandwidth feedback loop since not only the motion dynamics of the extruder (printhead) can be considered adequately linear (contrary to highly nonlinear extrusion dynamics) but

also all control process variables are sensed and computed in a real-time mode, (2) benefits from a vision-based control approach whose performance does not rely on a dynamic model.

In this paper, a real-time vision-based control of industrial manipulators for layer-width setting in concrete 3D printing applications is presented. In the control strategy, the width information of the printed layer is obtained and analyzed online during the robot motion through a vision system. This real-time information is related to the robot velocity, printhead outlet geometry shape and the flow rate of the building material extrusion. Simultaneously, a real-time velocity control approach is used to move a printhead toward a prescribed path. During the whole printing process, the building material was pumped to the printhead with a constant extrusion flow rate. Concisely, the real-time control approach adjusts the robot velocity to obtain the layer-width of desire based on the online vision feedback in a way that possible oncoming deformations and collapses do not appear in the printed object. The proposed approach allows to regulate the deposit speed and not the pump flow rate and thus to overcome the delay induced by the flow in the pipe and the rheological problems along this same pipe and the extrusion nozzle. While an acceptable layer width-setting for many users is generally going to be around the nozzle shape geometry with an approximate percent error of 20%, the main contributions of this work are presented as follows:

- Printing highly accurate rectangular bar-shaped layers with a width equal to the printhead outlet width;
- Printing accurate rectangular bar-shaped layers with a layer-width of desire in the range from -10 to 10 % of the printhead outlet width;
- Printing continuous and coherent rectangular bar-shaped layers in a way that discontinuities and buckles do not occur in the final printed structure.

In addition, for the purpose of planning the printing path properly and efficiently, a procedure framework for converting the CAD of the object to be printed to robot printing paths (numerical motion control system commands) is presented. Furthermore, a novel printhead with a rectangular nozzle cross-section is designed and developed in this work. The design of the printhead is the result of a design process aimed at solving all the constraints related to the robotization of extrusion-based additive manufacturing.

This paper is organized as follows: first, principals of the real-time vision-based control system are described in Section 2. In Section 3, the robotic concrete 3D printing platform is explained. The experimental tests and performance analyses are discussed in Section 4. Finally, in Section 5, conclusions are drawn.

2. Real-time vision-based control system

In this section, principals of the real-time vision-based control system of industrial manipulators for layer-width setting in concrete 3D printing applications, developed and proposed in this work, are explained.

2.1. Control system strategy overview

A block diagram of the real-time vision-based control system, proposed in this work, is shown in Fig. 2. Actually, the main idea is to regulate a printhead (extruder) motion velocity during the printing process to control the geometry based on a reference layer-width. On this basis, the real-time layer-width information is extracted through edge detection and layer-width calculation algorithms from a camera (vision system). Principally, the vision system has an important role in our concrete 3D printing robotic platform. That is, it directly affects the geometry accuracy and shaping quality of the printed object. Actually, the main application of the vision system in our system is to measure the width of the printed layer during the printing process. On this basis, the vision system grabs and analyzes the image data obtained from the vision sensor to detect edges of the printed layer and then compute the distance between the edges (layer-width) for each image frame. Consequently, the difference between the desired layer-width (reference) and output of the vision system is used as the input (error) of an industrial control system. Then, the industrial controller computes a control signal (u_c) which represents the velocity to be tracked by an industrial manipulator.

For preventing too fast and too slow motions of the printhead during the printing process due to security issues, a velocity limiter function is implemented to the control system. In fact, the velocity limiter function limits the velocity signal which is generated by the industrial controller and to be tracked by the robot within a defined range. That is, if the controller output signal exceeds either limit, the extruder velocity value remains at that limit.

While the extrusion flow rate is kept constant during the printing process, commands for generating switching on/off signals of the printhead and concrete pump are embedded in the main manipulator motion program algorithm running on the robot motion controller unit.

The rest of the paper will be evident from technical descriptions and details of the overall system in the next sections.

2.1.1. Edge detection and layer-width measurement algorithms

The most fundamental image analysis operation in this work is the edge detection algorithm as it is used to distinguish the margins of printed layers. Theoretically, an edge can be defined as a remarkable alternation in the gray-scale values between adjacent pixels in an image frame (Kwon and Ready, 2014). Edges have a tendency to occur at the boundary between two completely different portions of an image (region of interest (ROI)). Hence, the application of the edge detection algorithm in this work, developed in LabVIEW software, is to provide a limning of a scene by tracing and tracking down the edges (boundaries) of the printed bar-shaped layers among camera frames as shown in Fig. 3.

In order to calculate the distance between the marginal lines (layer edges) for measuring the width of the printed layer, a layer-width measurement algorithm is needed. Accordingly, for formulating the relation between features of an image frame and the layer-width, a corresponding schematic view of a printed layer segment is shown in Fig. 4. While (x_{A1}, y_{A1}), (x_{B1}, y_{B1}), (x_{A2}, y_{A2}) and (x_{B2}, y_{B2}) are beginning and ending coordinates of layer edges in ROI, (x_{m1}, y_{m1}) and (x_{m2}, y_{m2}) represent midpoints of layer edges and can be calculated as:

$$(x_{m1}, y_{m1}) = \left(\frac{x_{A1} + x_{B1}}{2}, \frac{y_{A1} + y_{B1}}{2}\right); \tag{1}$$

$$(x_{m2}, y_{m2}) = \left(\frac{x_{A2} + x_{B2}}{2}, \frac{y_{A2} + y_{B2}}{2}\right). \tag{2}$$

Therefore, we can find the layer-width by using the formula for the distance between two points as follows:

$$s_{lw} = \sqrt{(x_{m2} - x_{m1})^2 + (y_{m2} - y_{m1})^2} \tag{3}$$

where s_{lw} denotes the width value of the printed layer.

2.1.2. Camera calibration

Before any experiments or image analysis application that involves real world measurements, a camera calibration procedure is needed to make a correspondence between pixel units and physical units (millimeter in our case). In our experiment, a calibration check-board plate with a number of 20×20 [mm] panes simulates the working object (as shown in Fig. 5). More details for the calibration procedure can be found in Zhang (2000).

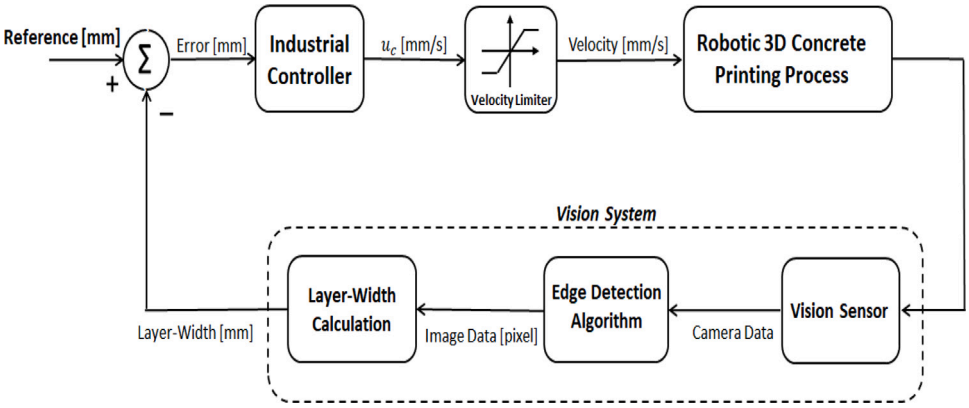

Fig. 2. Block diagram of control system strategy proposed in this study.

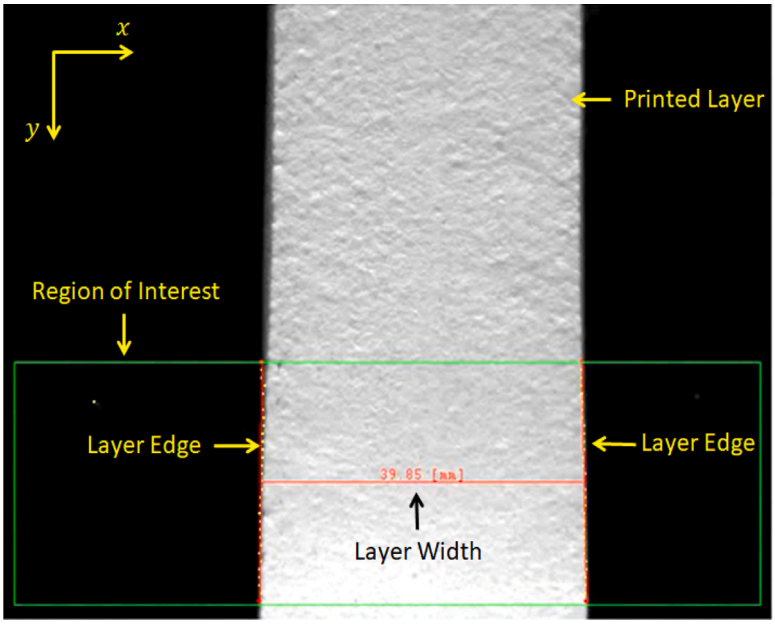

Fig. 3. An example of the edge detection technique applied on an image frame during the printing process with indications to some important features.

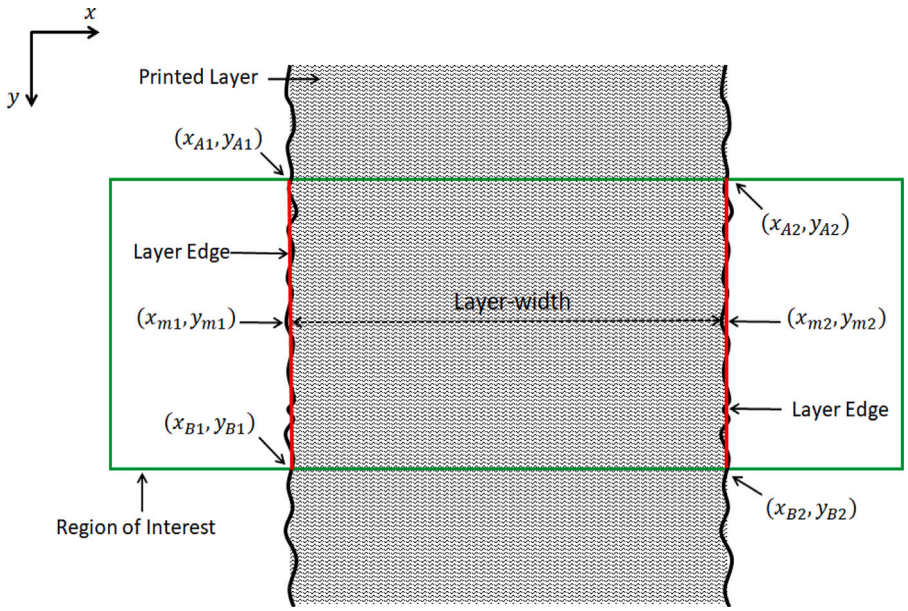

Fig. 4. Schematic view of the edge detection algorithm.

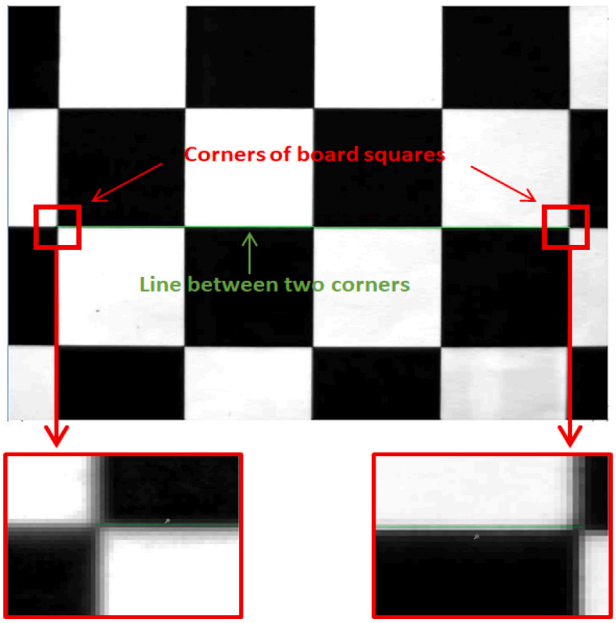

Fig. 5. Calibration check-board image captured by the camera during the calibration procedure with indications to some important features and two sub-images.

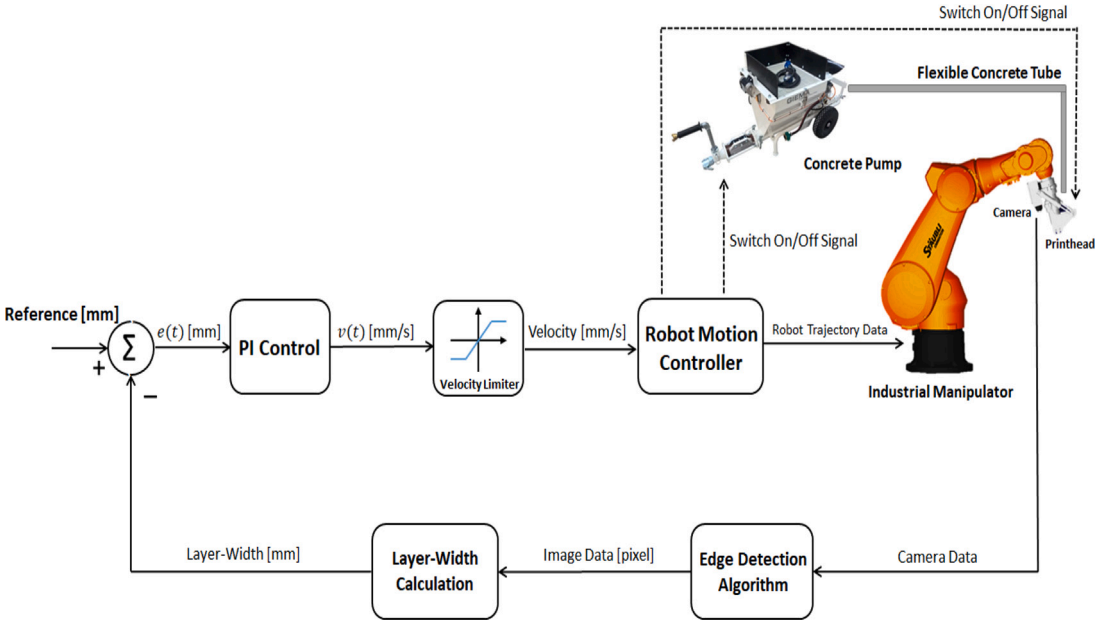

Fig. 6. Schematic diagram of real-time vision-based control.

2.2. Feedback control system

Fig. 6 shows a schematic diagram of the real-time vision-based control system strategy of an industrial manipulator for layer-width setting in concrete 3D printing applications, developed and proposed is this paper. While the feedback part of the control scheme contains the main vision system elements which were explained in earlier sections, the processing parts consisted mostly of the control system components that will be described in this section.

In our robotic 3D concrete printing process, each layer is printed by the printhead nozzle that extrudes the building material with a constant extrusion flow rate and moves on a predefined path. Correspondingly, by moving the nozzle along the pre-planned path during the printing process, the vision system calculates the layer-width from a vision sensor (camera) using image-processing techniques. In consequence, the difference between the desired layer-width (reference) and output of the vision system is fed as an input to a classical proportional integral (PI) controller. Then, the PI controller computes the control signal which represents the velocity to be tracked by the robot and can be expressed mathematically as follows:

$$v(t) = K_p e(t) + K_i \int e(t)dt \tag{4}$$

where $v(t)$ is the controller output and $e(t)$ defines the current controller error. K_p and K_i represent proportional and integral gains respectively, variable t is the instantaneous time and dt expresses the delta timing. Basically, the proportional controller is suited to increase the control signal for the same level of the error and the integral action tends to reduce the steady-state error (Shojaei Barjuei and Ortiz, 2021).

Principally, the stability of the robot motion controller unit during normal operation of the manipulator is assured by the manufacture.

Hence, the stability of the robot motion controller in combination with the outer loop is hardly affected as the data from the master controller (PI controller) are transmitted at a lower frequency (De Graaf et al., 2010; Barjuei et al., 2020).

As explained earlier, in order to consider some technical and security aspects during the printing experiments, a velocity limiter function is implemented to the control scheme. It is worth to mention that the smoothness of the robot motion depends mainly on the measured data. This is particularly relevant to the vision system where image frames of the printed layer are captured by the camera and corresponding measurements and image processing are carried out. If too noisy sensor data are used to be fed to the PI controller, oscillation in the velocity profile to be tracked and sent to robot motion controller may affect in the robot motion. These oscillations can result in discontinuities and buckles in printed layers. Consequently, some technical and theoretical aspects such as generating homogeneous light distribution and choosing a proper background in order to reduce the measurement noise should be considered in practice.

3. Robotic concrete 3D printing platform

In this section, explicit technical descriptions for the developed robotic concrete 3D printing platform are given.

3.1. System descriptions

The real-time vision-based control of industrial manipulators for layer-width setting in concrete 3D printing applications developed in this study mainly consists of a 6-axis industrial manipulator produced by Staübli robotics (TX200 industrial robot with a load capacity of 130 [kg]), a TP5 Giema electric pump designed for mortar/render application (maximum pressure of 20 [bar], maximum flow rate of 40 [$\mathrm{l\,min^{-1}}$]), a printhead consisting of a rectangular nozzle outlet with a pneumatic shut-off system and a real-time vision-based control system.

A schematic view of the real-time vision-based 3D printing robotic system, developed and proposed in this study, is shown in Fig. 7. As it can be seen, the building material is transferred by a pumping operation through an electric pump in order to be extruded through a printhead. On the other hand, an industrial camera (optical measuring instrument) is mounted with the printhead to the end-effector of the manipulator while it is connected to a master controller (Compact Rio (cRIO-9035), manufactured by National Instrument, and programming with LabVIEW software Klinger, 2003). The images acquired by the camera are sent to the master controller for a real-time machine vision processing. The vision system output is then sent to an embedded control algorithm which works in parallel with the vision system and generates the reference motion velocity to be tracked by the robot. The master controller is also connected to a robot motion controller (Staübli CS8C HP) and a supervisory computer for data transmissions, process monitoring and further data analysis. During 3D printing experiments, the building material is pumped to the printhead with a constant extrusion flow rate through a flexible concrete tube by the electric pump. The manipulator moves the printhead along the predefined printing path with the velocity set by the industrial control system based on the information receiving from the vision system. It should be also mentioned that switching off/on of the printhead is done through pneumatic actuators and by a control program which is developed with VAL3 language-Staübli and embedded in the main manipulator program running on the robot motion controller (Staübli CS8C HP).

To guarantee the stability of the closed-loop control system, system time delays (communication time, image acquisition time and image processing time), which are parts of the feedback loop, need to be accurately known. Practically, a typical frequency bandwidth for the closed-loop system of these type of robotic manipulator motion controllers (Staübli CS8C HP) is about 10 [Hz]. In our application, the PI controller is developed with LabVIEW software and running on the master controller (CompactRIO) with a sampling time of 0.1 [s]. The master controller communicates with the robot controller through a TCP/IP protocol with a sample frequency of 5 [Hz]. This implies that the data transmission to the robot motion controller for a typical instantaneous value of the velocity signal by the PI controller is done every 0.2 [s] which is lower than the robot controller working frequency. Therefore, it can be inferred that the stability of our closed-loop control system is guaranteed respect to the system operating frequency bandwidth.

3.2. Printhead design

In order to obtain a successful print, the printhead design plays an important role in shaping the final structure. Fig. 8 shows a prototype design of the printhead used for the experimental validation including a rectangular nozzle outlet, a pneumatic closing system, a feeding part and a part being connected to the flange of the manipulator.

In order to achieve rectangular shaped extrudate, the material flow path gradually changes from a circular section of diameter 32 [mm] to 42×20 [mm] rectangular section while keeping a constant cross-section area. The printhead is fixedly supported by the robot flange. The nozzle is collinear with the sixth robot axis which allows keeping the nozzle tangent to the print path. The nozzle is made of two half-shells to be fixedly clamped to the connection part and also to facilitate the cleaning. To prevent the supply hose from curling up when tracking the printing path, the part connected to the pipe may be freely turned about the sixth robot axis. The pivot link is provided by two bronze bearings. The sealing is ensured by two lip seals in the bearing housing. The closing system is made of a pressure-resistant closure plate operated by two pneumatic cylinders directly controlled by solenoid valves located in the robot arm.

3.3. Vision system

For hardware, the overall system is composed of an industrial monochromatic camera (Basler acA720) with a frame rate of 291 [fps] and an imaging lens (Fujinon HF16HA-1S). While color and high-speed cameras are used in color and object inspection applications respectively; monochromatic cameras are an appropriate solution in shape detection or geometrical object matching tasks. The camera communicates with the main processing unit (master controller) through a Transmission Control Protocol/Internet Protocol (TCP/IP). On the other hand, the software system includes the edge detection and measuring distance algorithms which are developed with LabVIEW software and running on the master controller (CompactRIO) with a sampling rate of 10 [Hz].

3.4. CAD to robot path

In this section, the process framework for converting a computer-aided design (CAD) to robot printing paths is explained. As the first step, the information of the target object should be expressed as robot motion data and commands in original files format of the robot motion controller unit. In our application, RoboDK software (Pollák et al., 2019) offers the ability to simulate and convert an initial graphics exchange specification (IGES) file defining the trajectories to follow into Staübli robot controller programming language (VAL3) files with automatic optimization of the robotic manipulator arm motion while ensuring trouble-free operation without collisions with the environment. Finally, VAL3 files are compiled and transferred to the robot motion controller unit (Staübli CS8C HP) via Staübli robotic suite (SRS) (Alhama Blanco et al., 2018) which is a software workbench for offline development and online operations. Fig. 9 shows the sequence diagram of steps to convert the drawing design defined with CATIA software (Tickoo, 2018)into the robot motion controller language (.pgx file).

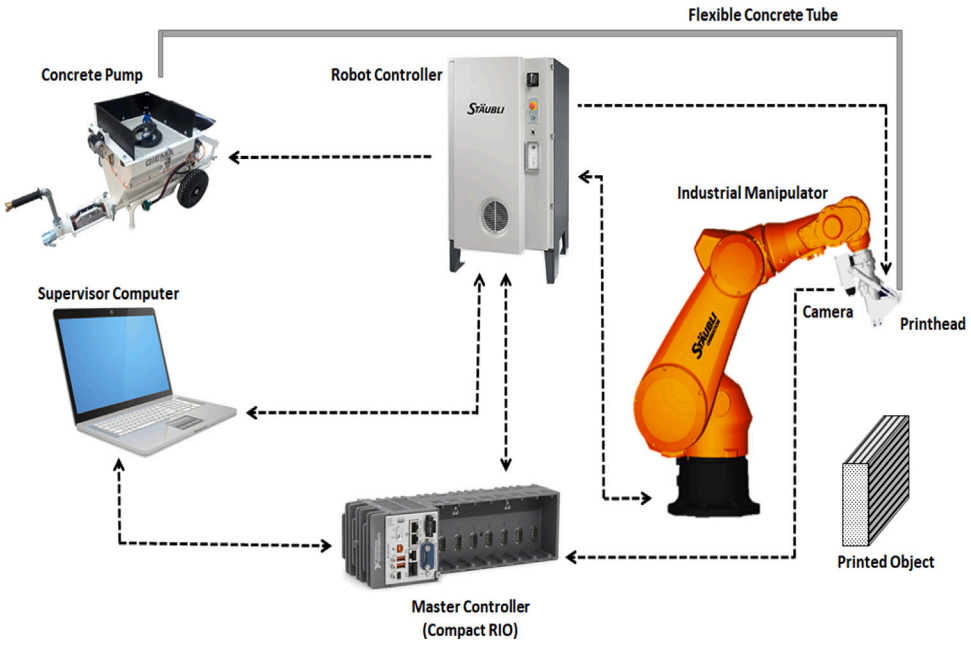

Fig. 7. Schematic view of the real-time vision-based concrete 3D printing robotic system.

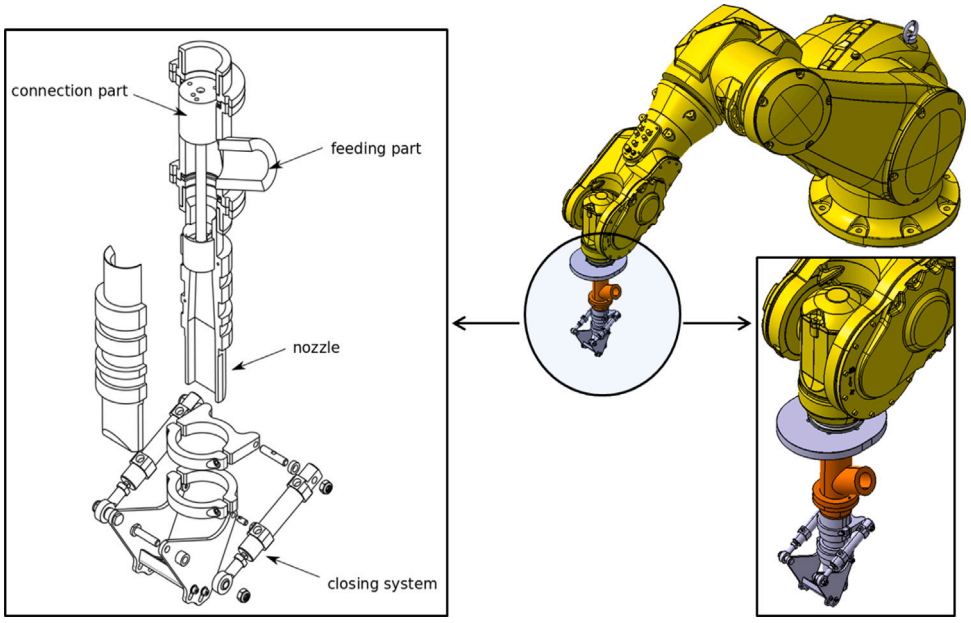

Fig. 8. Printhead prototype design which is mounted on an industrial manipulator with an exploded-view drawing and a close-up view.

4. Experimental tests and results

The performance and effectiveness of the proposed real-time vision-based control of industrial manipulators for layer-width setting in concrete 3D printing applications are evaluated and verified through some experimental tests. The robotic concrete 3D printing workcell for carrying out the experimental tests in this work is shown in Fig. 10. Accordingly, the implementation and results obtained from the experimental tests are reported and discussed in this section.

4.1. Building material

The building material used in experiments is a mixture of 50% sand with a grain size ranging from 0 to 1 [mm], 25% limestone filler (Betocarb Omya) with a particle size in the range of $0-80$ [μm] and 25% kaolin (Polwhite EB) with a high quality medium particle size ($0-80$ [μm]). The water content of the material (water to solid particles mass ratio) is 18%.

This material demonstrates a rheological behavior close to cement-based mortar or raw earth materials, used for construction 3d printing applications (Perrot et al., 2016a), with a shear threshold (yield stress) of 1 kPa. This threshold allows the material to be pumpable and to have sufficient shape resistance at the output of the printhead nozzle. In fact, the reusability and great stability over time are the main reasons to choose this material for practical experiments of this study.

4.2. 3D printed objects

In experimental tests, four straight single layers with different wideness but the same length are printed by means of an unique printhead

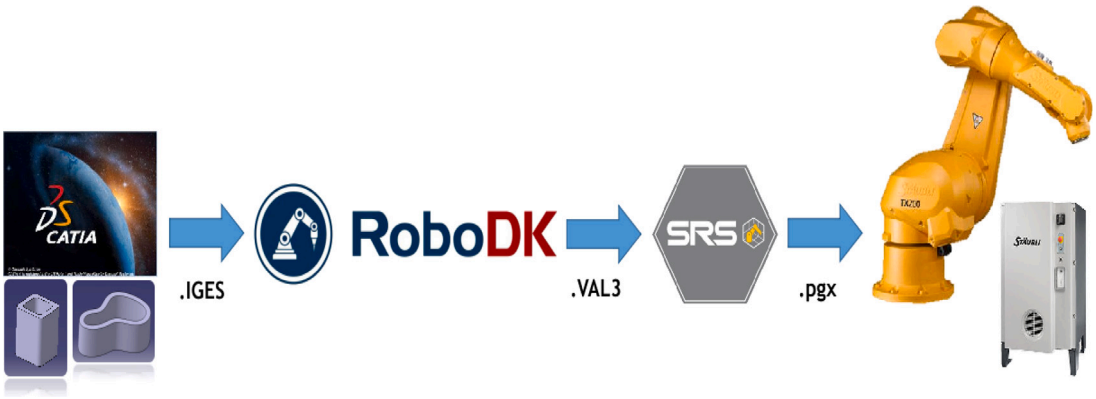

Fig. 9. Sequence diagram for converting 3D drawing model to Staübli robot motion commands.

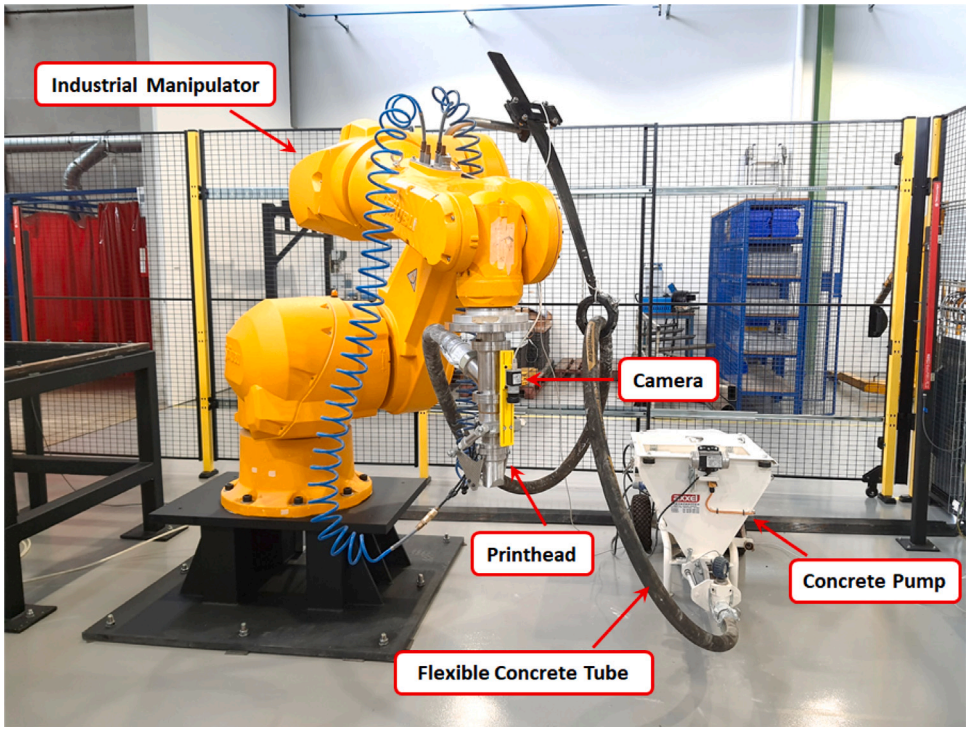

Fig. 10. Robotic concrete 3D printing workcell with indications to some main components.

with a constant rectangular nozzle. In continue, an additional experimental test is carried out to demonstrate the accuracy and responsiveness of the control system by printing (stacking) two layers with the same width above another. The printed layers obtained from the experimental tests are shown in Fig. 11. Although the straight-shape layers are used as the target objects to be printed in our experiments, the proposed control system can be extended and implemented to any object that are kinematically feasible for the robotic manipulator. It is worth to mention that the developed edge detection algorithm in this work is very sensitive to homogeneous (uniform) light distribution so it is important to consider and implement practically this fact during the printing process.

For the first experiment, four straight single layers with a length of 2 [m] and wide of 44, 42, 40 *and* 38 [mm] are printed by means of the same printhead with a constant rectangular nozzle (42×22 [mm]). During the printing process, the extrusion rate was kept constant at 3.8 [$\mathrm{l\,min^{-1}}$]. While the trajectory information and corresponding motion commands to be executed by the manipulator are stored and run on the robot motion control unit, the printhead motion speed is controlled through the PI controller based on the vision system feedback in a velocity range of $60 - 150$ [$\mathrm{mm\,s^{-1}}$]. Examples of image frames from printed layers, captured and processed by the vision system, during experimental tests are illustrated in Fig. 12. In order to prevent undesirable influences by unwanted alterations of data from the vision system, the printhead traveling speed was kept constant at 112.5 [$\mathrm{mm\,s^{-1}}$] at the beginning of each layer (20 [cm]).

4.3. PI control tuning

PI controller tuning involves setting the two proportional and integral gains. The optimal value of these control gains is determined throughout the experiment by setting $K_p = 0.75$ [$\mathrm{s^{-1}}$] and $K_i = 0.6$ [$\mathrm{s^{-2}}$] to achieve a fast rise time and small steady-state error.

4.3.1. Measurement accuracy

Regarding to our calibration experiment (explained in Section 2.1.2), the equivalency value for converting image pixels to millimeters is 0.126582 [mm/pixel] for our system. It should be noted that the

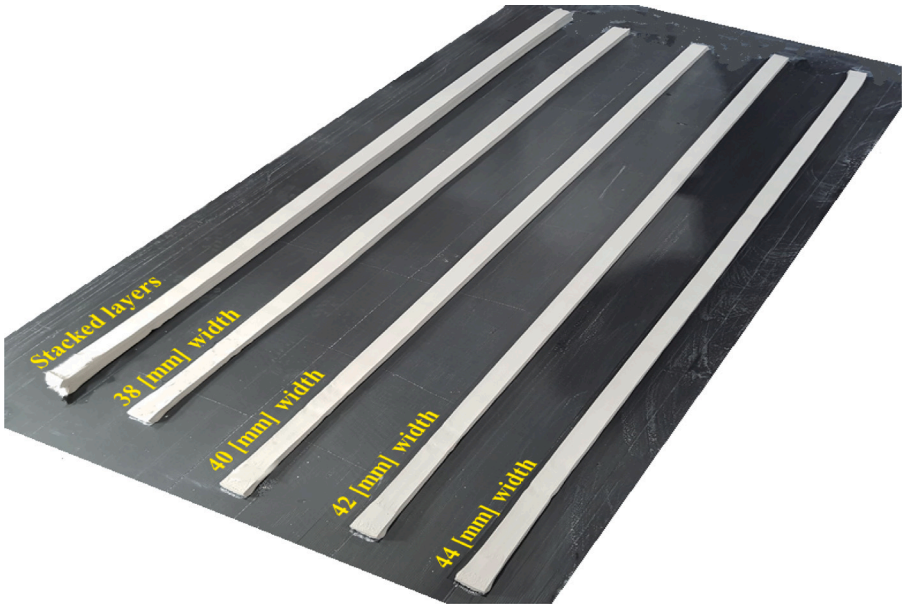

Fig. 11. Printed layers with width of 44, 42, 40 *and* 38 [mm] and two stacked layers.

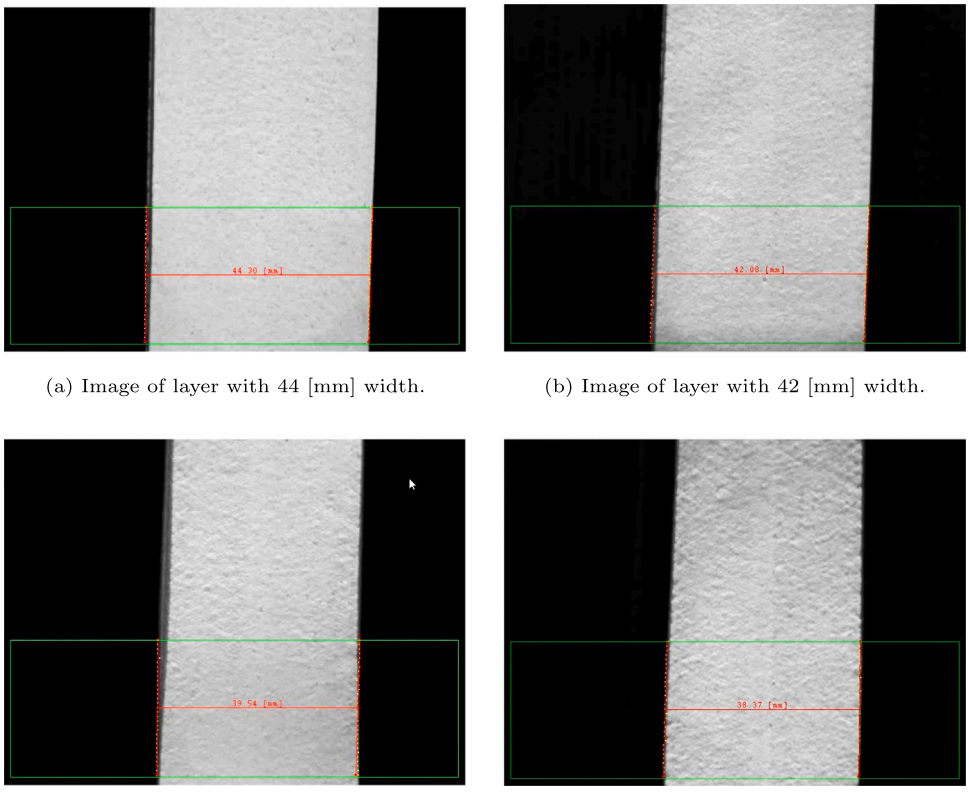

(a) Image of layer with 44 [mm] width.

(b) Image of layer with 42 [mm] width.

(c) Image of layer with 40 [mm] width.

(d) Image of layer with 38 [mm] width.

Fig. 12. Examples of image frames from printed layers with the wide of 44, 42, 40 *and* 38 [mm] during printing experiments.

equivalency value will remain valid until the distance between the camera and printed layer to be measured (stand-off distance (SOD)) is constant. Consequently, the printed layer thickness is estimated as the wide of the printhead rectangular nozzle (Roussel, 2018) and it can be also taken into account as the elevation-distance for the printhead (robot end-effector) after printing termination of each layer. This assumption could be sufficiently adapted to our application as much as the thickness deformation of the printed layer due to the gravity effect is very small.

In order to obtain the effect of alternations in the distance between the camera and object to be measured, an experimental test was carried out. In this test, the camera was calibrated initially in a constant distance from the object to be measured. Then, while the camera was vertically located to different constant distance from the reference (calibration) object, the corresponding measurements were registered

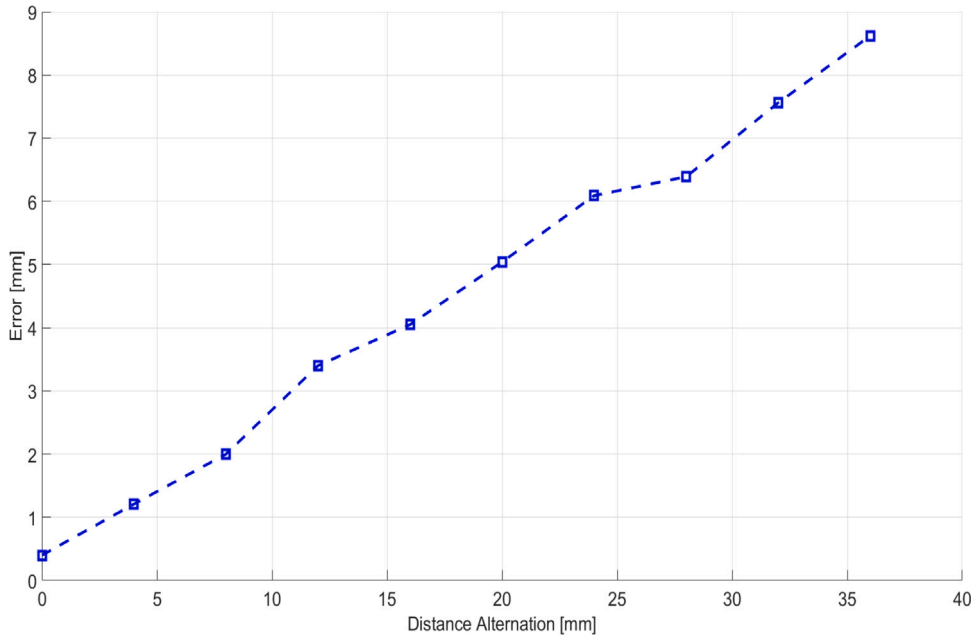

Fig. 13. Error due to changes in the distance considered for the camera calibration procedure.

Table 1
Errors on wideness measurements of printed layers with layer-width of 44, 42, 40 *and* 38 [mm].

Layer-Width	Mean Error	Root-Mean-Square Error (RMSE)
44 [mm]	1.3 [mm]	1.9 [mm]
42 [mm]	0.8 [mm]	1.3 [mm]
40 [mm]	0.4 [mm]	0.6 [mm]
38 [mm]	0.5 [mm]	0.5 [mm]

Table 2
Average velocities of the printhead for printing layers with 44, 42, 40 *and* 38 [mm] width.

Layer-Width	Average Velocity
44 [mm]	73.8 [mm s^{-1}]
42 [mm]	81.1 [mm s^{-1}]
40 [mm]	96.6 [mm s^{-1}]
38 [mm]	115.8 [mm s^{-1}]

and recorded. The outcome of the test is an error-distance alternation curve which is plotted in Fig. 13. From this figure, it can be concluded that a variation of 5 [mm] in the distance between the camera and object (SOD) to be measured causes a measurement error of 1.2 [mm] and this error grows up almost linearly by increasing the distance between the camera and object to be measured.

4.4. Results and discussion

The wideness measurement of four single printed layers with 44, 42, 40 *and* 38 [mm] width by the vision system during the printing process are shown in Fig. 14. It can be clearly seen that the developed control framework tracks the desire reference efficiently for all printed layers and the control approach is well suited for layer-width setting in robotic concrete 3D printing applications. Accordingly, Fig. 15 illustrates the error on the printed layers. As it can be inferred, the error on each layer converges to zero as long as the printhead moves from the starting point. The information related to mean and root-mean-square errors on each printed layer is reported in Table 1.

By comparing the results from Fig. 14 and Fig. 15, it can be seen that the proposed control approach not only provides a good capability to creating highly accurate rectangular bar-shaped layers with a wideness almost near to the width of the printhead nozzle cross-section, but also it gives a possibility to print accurate square bar-shaped layers with layer-width of desire in the range from −10 to 10 % of the printhead nozzle cross-section width.

Another interesting finding from Fig. 14 and Fig. 15 is different time periods for the printing process of the layers with the same length (2 [m]) and different width (44, 42, 40 *and* 38 [mm]). Given this, it can be deducted that requiring specific printing velocity for each layer-width setting results in different time periods. Accordingly, Fig. 16 shows the printhead (manipulator end-effector) velocity generated by the PI control and tracked by the robot during printing experiments of the four single layers with 44, 42, 40 *and* 38 [mm] width. As can be seen from Fig. 16, the effect of an increase in layer-width is a lower printhead velocity, and vice versa. For instance, whereas the printhead moves with the highest velocity for printing the 38 [mm] layer-width, the lowest printhead velocity is for printing the layer with 44 [mm] width. Average velocities of the printhead for printing experiments of each layer are reported in Table 2. It is also worth mentioning that the notable different between the velocity of the robot and the one generated by the PI controller in Fig. 16(d) (fastest motion) is because of the motion constrains embedded in the robot motion control unit by the manufacture for security and safety aspects in industrial manipulators.

One way to investigate the accuracy and responsiveness of the proposed control approach for printing continuous and coherent layers in this work, is to stacked layers centrally above another with a same width. Therefore, apart of former experiments, two layers with a width of 38 [mm] and the same length (2 [m]) are printed centrally above another. The stacked layers obtained from our experimental test are illustrated in Fig. 17. It can be clearly seen that a very good contact with a high accuracy between layers exists. This means that there is an excellent level of continuity and coherency for printed layers in absence of any possible oncoming deformations and collapses. The result highlights a great improvement in the compactness and mechanical strength of the final printed structure.

Consequently, results of the experiments found clear support for accuracy and responsiveness of the proposed control approach for layer-width setting in robotic construction 3D printers applications. As formerly mentioned, during the printing process, the height of the

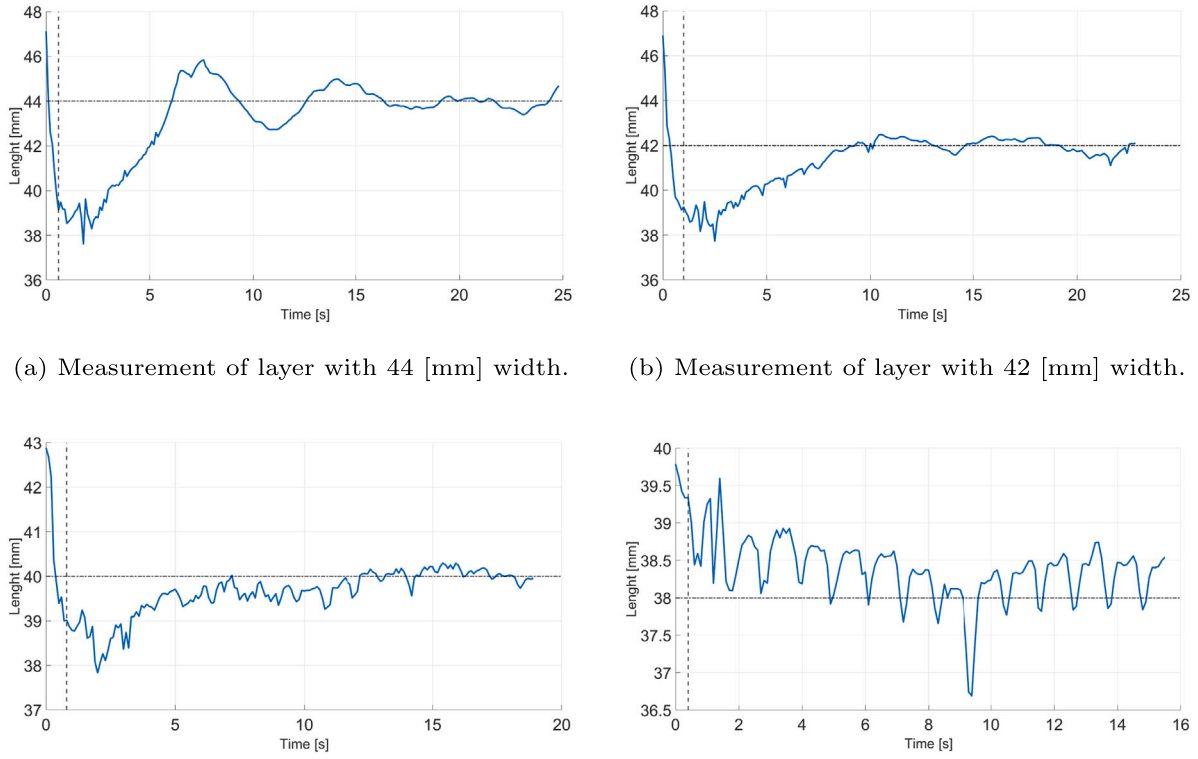

(a) Measurement of layer with 44 [mm] width.

(b) Measurement of layer with 42 [mm] width.

(c) Measurement of layer with 40 [mm] width.

(d) Measurement of layer with 38 [mm] width.

Fig. 14. Wideness measurement of four single printed layers with layer-width of 44, 42, 40 *and* 38 [mm] by the vision system during printing experiments. While vertical dash-lines represent the activation point of the control system, horizontal dash-lines are the desired width reference for the layer to be printed.

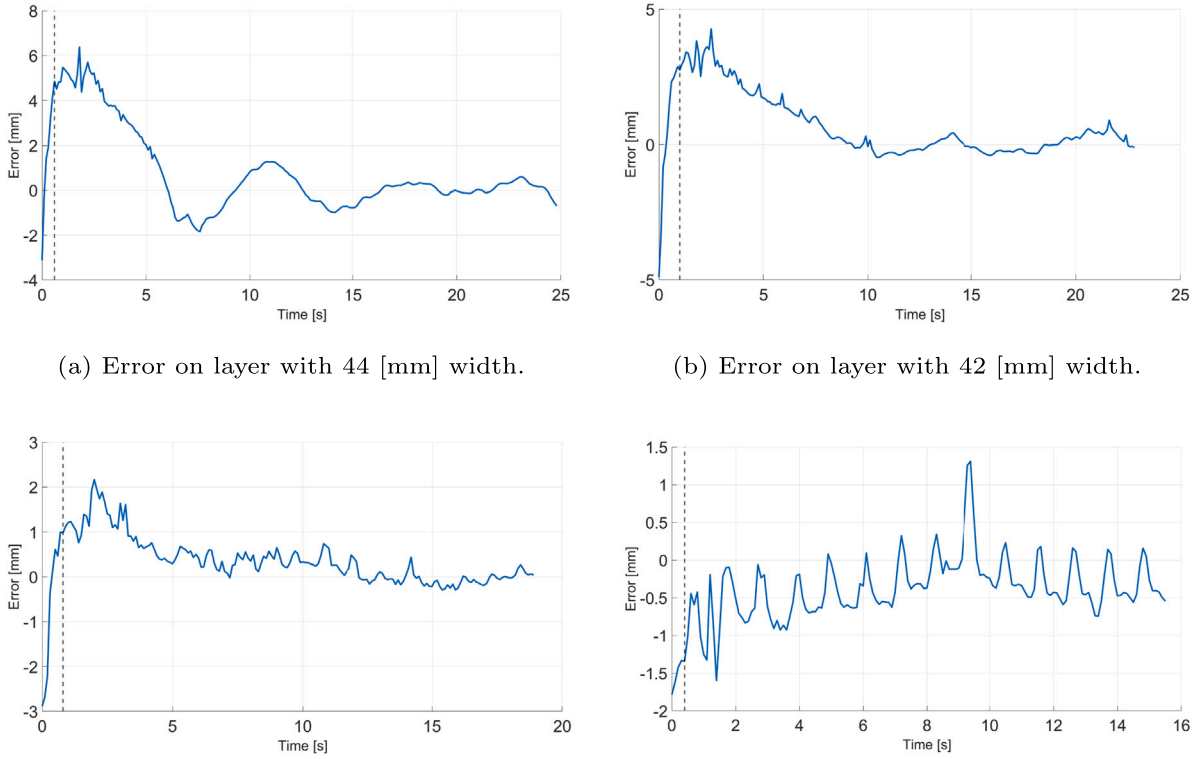

(a) Error on layer with 44 [mm] width.

(b) Error on layer with 42 [mm] width.

(c) Error on layer with 40 [mm] width.

(d) Error on layer with 38 [mm] width.

Fig. 15. Error on the wideness of printed layers with layer-width of 44, 42, 40 *and* 38 [mm]. Vertical dash-lines represent the activation point of the control system.

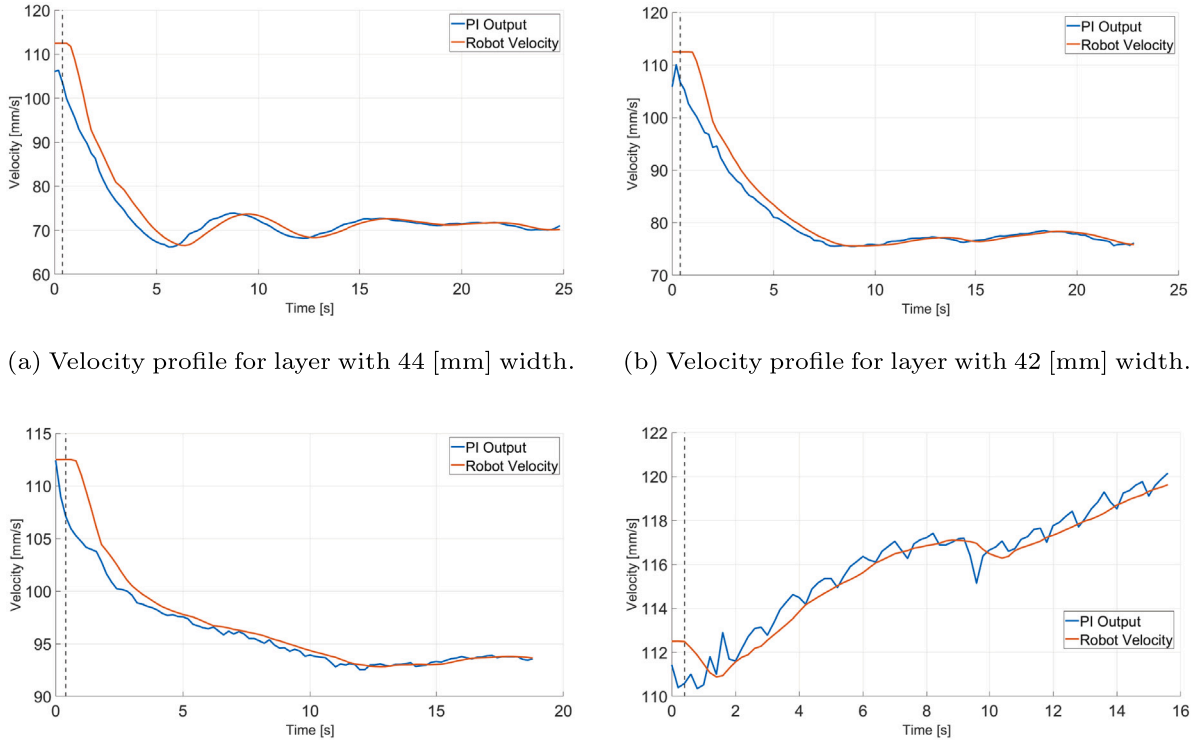

(a) Velocity profile for layer with 44 [mm] width.

(b) Velocity profile for layer with 42 [mm] width.

(c) Velocity profile for layer with 40 [mm] width.

(d) Velocity profile for layer with 38 [mm] width.

Fig. 16. The velocity generated by the PI controller and tracked by the robot for printing layers with layer-width of 44, 42, 40 *and* 38 [mm]. Vertical dash-lines represent the activation point of the control system.

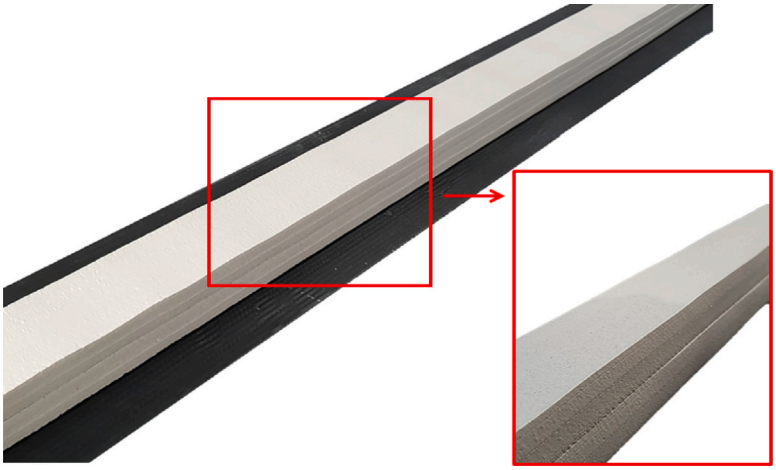

Fig. 17. Stacked layers in far and close-up views.

printhead above the printed layer is almost equal to the printhead nozzle outside width. This results in a smooth deposition of the printed layers, and avoids interaction between the printed layers and the printhead nozzle (Bos et al., 2016).

5. Conclusion

In this work, a novel real-time vision-based control of industrial manipulators for producing rectangular bar-shaped layers with a desired width in concrete 3D printing applications is developed and presented. Although the control approach is evaluated experimentally by printing straight layers, it can be extended and implemented on objects with various layer geometries which are kinematically feasible for the robot and being made of different materials.

A printhead with a constant rectangular nozzle and pneumatic shut-off system was designed and developed to provide a smooth flow rate of the building material and avoid collisions between the robotic manipulator and flexible concrete tube. After the development of the vision-based control system, evaluating the reliability and responsiveness of the proposed control system are carried out through some experimental tests. In these experiments, four single bar-shaped layers with different widths but the same length were printed. In continue, two straight layers with the same dimension were stacked above another. Printing experiments were conducted by means of an unique printhead with a constant rectangular nozzle and the data representing the quality of printing was recorded.

The results achieved in this work from the proposed control framework are satisfactory and illustrate a fast and accurate response in terms

of producing continues and coherent cement-based layers. The width of the printed layers can not only be nearly equal to the width of the printhead nozzle cross-section with a mean error of 0.8 [mm], but also it can be in the range of −10−10 % of the nozzle width based on the user's choice with a maximum mean error of 1.3 [mm]. Overall, the presented experimental results demonstrate a high accuracy, effectiveness and responsiveness of the proposed real-time vision-based control approach. It was shown that the proposed control approach could improve significantly the quality of the robotic 3D printing process for building and construction purposes. In particular, our findings and results cast a new light on layer-width setting in robotic 3D construction printers.

In summary, this paper introduced and proposed a novel real-time vision-based control of industrial manipulators for layer-width setting in concrete 3D printing applications as a promising approach to address challenges facing robotic technologies in cement-based building construction for implying great potentials and opening up new avenues of high precision and accurate design possibilities.

Future research will be devoted to print complex-shaped objects with different layer geometries containing curved and corners layers which are vastly used in building structure by employing control techniques based on 3D geometry.

Declaration of competing interest

The authors declare that they have no known competing financial interests or personal relationships that could have appeared to influence the work reported in this paper.

Acknowledgment/funding

This project is funded by the European Community (FEDER funding) and Brittany Region, France (Research project R3DPRINT, SAD "Stratégie d'Attractivité Durable").

References

Albar, A., Chougan, M., Al-Kheetan, M.J., Swash, M.R., Ghaffar, S.H., 2020. Effective extrusion-based 3D printing system design for cementitious-based materials. Results Eng. 6, 100135.

Alhama Blanco, P.J., Abu-Dakka, F.J., Abderrahim, M., 2018. Practical use of robot manipulators as intelligent manufacturing systems. Sensors 18 (9), 2877.

Armstrong, A.A., Alleyne, A.G., 2021. A multi-input single-output iterative learning control for improved material placement in extrusion-based additive manufacturing. Control Eng. Pract. 111, 104783.

Asprone, D., Auricchio, F., Menna, C., Mercuri, V., 2018. 3D Printing of reinforced concrete elements: Technology and design approach. Constr. Build. Mater. 165, 218–231.

Bard, J., Cupkova, D., Washburn, N., Zeglin, G., 2018. Robotic concrete surface finishing: a moldless approach to creating thermally tuned surface geometry for architectural building components using profile-3D-printing. Constr. Robot. 2 (1–4), 53–65.

Barjuei, E.S., Ardakani, M.M.G., Caldwell, D.G., Sanguineti, M., Ortiz, J., 2020. Optimal selection of motors and transmissions in back-support exoskeleton applications. IEEE Trans. Med. Robot. Bionics 2 (3), 320–330.

Barjuei, E.S., Boscariol, P., Vidoni, R., Gasparetto, A., 2016. Robust control of three-dimensional compliant mechanisms. J. Dyn. Syst. Meas. Control 138 (10), 101009.

Barjuei, E.S., Gasparetto, A., 2015. Predictive control of spatial flexible mechanisms. Int. J. Mechan. Control (JoMaC) 16 (01), 85–96.

Bos, F., Wolfs, R., Ahmed, Z., Salet, T., 2016. Additive manufacturing of concrete in construction: potentials and challenges of 3D concrete printing. Virtual Phys. Prototyp. 11 (3), 209–225.

Bozkurt, Y., Karayel, E., 2021. 3D Printing technology; methods, biomedical applications, future opportunities and trends. J. Mater. Res. Technol. 14, 1430–1450.

Buswell, R.A., De Silva, W.L., Jones, S.Z., Dirrenberger, J., 2018. 3D Printing using concrete extrusion: A roadmap for research. Cem. Concr. Res. 112, 37–49.

Carloni, D., Zhang, G., Wu, Y., 2021. Transparent alumina ceramics fabricated by 3D printing and vacuum sintering. J. Eur. Ceram. Soc. 41 (1), 781–791.

Carneau, P., Mesnil, R., Ducoulombier, N., Roussel, N., Baverel, O., 2020. Characterisation of the layer pressing strategy for concrete 3D printing. In: RILEM International Conference on Concrete and Digital Fabrication. Springer, pp. 185–195.

Chan, H.K., Griffin, J., Lim, J.J., Zeng, F., Chiu, A.S., 2018. The impact of 3D printing technology on the supply chain: Manufacturing and legal perspectives. Int. J. Prod. Econ. 205, 156–162.

Cheng, Y., Jafari, M.A., 2008. Vision-based online process control in manufacturing applications. IEEE Trans. Autom. Sci. Eng. 5 (1), 140–153.

Comminal, R., Serdeczny, M.P., Pedersen, D.B., Spangenberg, J., 2019. Motion planning and numerical simulation of material deposition at corners in extrusion additive manufacturing. Addit. Manuf. 29, 100753.

Comminal, R., da Silva, W.R.L., Andersen, T.J., Stang, H., Spangenberg, J., 2020. Modelling of 3D concrete printing based on computational fluid dynamics. Cem. Concr. Res. 138, 106256.

Costanzi, C.B., Ahmed, Z., Schipper, H.R., Bos, F., Knaack, U., Wolfs, R., 2018. 3D Printing concrete on temporary surfaces: The design and fabrication of a concrete shell structure. Autom. Constr. 94, 395–404.

De Graaf, M., Aarts, R., Jonker, B., Meijer, J., 2010. Real-time seam tracking for robotic laser welding using trajectory-based control. Control Eng. Pract. 18 (8), 944–953.

Deuser, B.K., Tang, L., Landers, R.G., Leu, M.C., Hilmas, G.E., 2013. Hybrid extrusion force-velocity control using freeze-form extrusion fabrication for functionally graded material parts. J. Manuf. Sci. Eng. 135 (4).

Ducoulombier, N., Mesnil, R., Carneau, P., Demont, L., Bessaies-Bey, H., Caron, J.-F., Roussel, N., 2021. The slugs-test for extrusion-based additive manufacturing: Protocol, analysis and practical limits. Cem. Concr. Compos. 121, 104074.

Greeff, G.P., Schilling, M., 2017. Closed loop control of slippage during filament transport in molten material extrusion. Addit. Manuf. 14, 31–38.

Hoffmann, M., Skibicki, S., Pankratow, P., Zieliński, A., Pajor, M., Techman, M., 2020. Automation in the construction of a 3D-printed concrete wall with the use of a lintel gripper. Materials 13 (8), 1800.

Hsiang Loh, G., Pei, E., Gonzalez-Gutierrez, J., Monzón, M., 2020. An overview of material extrusion troubleshooting. Appl. Sci. 10 (14), 4776.

Jo, J.H., Jo, B.W., Cho, W., Kim, J.-H., 2020. Development of a 3D printer for concrete structures: laboratory testing of cementitious materials. Int. J. Concr. Struct. Mater. 14 (1), 1–11.

Kazemian, A., Yuan, X., Davtalab, O., Khoshnevis, B., 2019. Computer vision for real-time extrusion quality monitoring and control in robotic construction. Autom. Constr. 101, 92–98.

Khan, M.S., Sanchez, F., Zhou, H., 2020. 3-D printing of concrete: beyond horizons. Cem. Concr. Res. 133, 106070.

Khoshnevis, B., 2004. Automated construction by contour crafting—related robotics and information technologies. Autom. Constr. 13 (1), 5–19.

Klinger, T., 2003. Image Processing with LabVIEW and IMAQ Vision. Prentice Hall Professional.

Kwon, K.-S., Ready, S., 2014. Practical Guide to Machine Vision Software: an Introduction with Labview. John Wiley & Sons.

Labonnote, N., Rønnquist, A., Manum, B., Rüther, P., 2016. Additive construction: State-of-the-art, challenges and opportunities. Autom. Constr. 72, 347–366.

Lao, W., Tay, D.Y.W., Quirin, D., Tan, M.J., 2018. The effect of nozzle shapes on the compactness and strength of structures printed by additive manufacturing of concrete. In: Proceedings of the 3rd International Conference on Progress in Additive Manufacturing. Pro-AM 2018, Singapore, pp. 14–17.

Lim, J.H., Weng, Y., Pham, Q.-C., 2020. 3D printing of curved concrete surfaces using adaptable membrane formwork. Constr. Build. Mater. 232, 117075.

Lu, B., Weng, Y., Li, M., Qian, Y., Leong, K.F., Tan, M.J., Qian, S., 2019. A systematical review of 3D printable cementitious materials. Constr. Build. Mater. 207, 477–490.

Lu, L., Zheng, J., Mishra, S., 2014. A model-based layer-to-layer control algorithm for ink-jet 3D printing. In: Dynamic Systems and Control Conference, Vol. 46193. American Society of Mechanical Engineers, V002T35A001.

Mazhoud, B., Perrot, A., Picandet, V., Rangeard, D., Courteille, E., 2019. Underwater 3D printing of cement-based mortar. Constr. Build. Mater. 214, 458–467.

Mechtcherine, V., Bos, F.P., Perrot, A., da Silva, W.L., Nerella, V., Fataei, S., Wolfs, R.J., Sonebi, M., Roussel, N., 2020. Extrusion-based additive manufacturing with cement-based materials–production steps, processes, and their underlying physics: A review. Cem. Concr. Res. 132, 106037.

Nematollahi, B., Xia, M., Sanjayan, J., 2017. Current progress of 3D concrete printing technologies. In: ISARC. Proceedings of the International Symposium on Automation and Robotics in Construction, Vol. 34. IAARC Publications.

Nerella, V., Näther, M., Iqbal, A., Butler, M., Mechtcherine, V., 2019. Inline quantification of extrudability of cementitious materials for digital construction. Cem. Concr. Compos. 95, 260–270.

Panda, B., Noor Mohamed, N.A., Paul, S.C., Bhagath Singh, G., Tan, M.J., Šavija, B., 2019. The effect of material fresh properties and process parameters on buildability and interlayer adhesion of 3D printed concrete. Materials 12 (13), 2149.

Paolini, A., Kollmannsberger, S., Rank, E., 2019. Additive manufacturing in construction: A review on processes, applications, and digital planning methods. Addit. Manuf. 30, 100894.

Park, C.Y., Jung, M.G., Kim, H.Y., Lee, M.C., 2017. Development of 3D printing simulator nozzle system using pid control for building construction. In: 2017 14th International Conference on Ubiquitous Robots and Ambient Intelligence. URAI, IEEE, pp. 368–369.

Perrot, A., Jacquet, Y., Rangeard, D., Courteille, E., Sonebi, M., 2020. Nailing of layers: a promising way to reinforce concrete 3D printing structures. Materials 13 (7), 1518.

Perrot, A., Rangeard, D., Courteille, E., 2018. 3D Printing of earth-based materials: Processing aspects. Constr. Build. Mater. 172, 670–676.

Perrot, A., Rangeard, D., Levigneur, A., 2016a. Linking rheological and geotechnical properties of kaolinite materials for earthen construction. Mater. Struct. 49 (11), 4647–4655.

Perrot, A., Rangeard, D., Pierre, A., 2016b. Structural built-up of cement-based materials used for 3D-printing extrusion techniques. Mater. Struct. 49 (4), 1213–1220.

Pollák, M., Kaščak, J., Telišková, M., Tkáč, J., 2019. Design of the 3D printhead with extruder for the implementation of 3D printing from plastic and recycling by industrial robot. TEM J. 8 (3), 709.

Reinold, J., Nerella, V.N., Mechtcherine, V., Meschke, G., 2022. Extrusion process simulation and layer shape prediction during 3D-concrete-printing using the particle finite element method. Autom. Constr. 136, 104173.

Roussel, N., 2018. Rheological requirements for printable concretes. Cem. Concr. Res. 112, 76–85.

Rushing, T.S., Stynoski, P.B., Barna, L.A., Al-Chaar, G.K., Burroughs, J.F., Shannon, J.D., Kreiger, M.A., Case, M.P., 2019. Investigation of concrete mixtures for additive construction. In: 3D Concrete Printing Technology. Elsevier, pp. 137–160.

Shojaei Barjuei, E., Ortiz, J., 2021. A comprehensive performance comparison of linear quadratic regulator (lqr) controller, model predictive controller (mpc), h_∞ loop shaping and μ-synthesis on spatial compliant link-manipulators. Int. J. Dynam. Control 9, 121–140.

Sotorrío Ortega, G., Alonso Madrid, J., Olsson, N.O., Tenorio Ríos, J.A., 2020. The application of 3D-printing techniques in the manufacturing of cement-based construction products and experiences based on the assessment of such products. Buildings 10 (9), 144.

Tho, T.P., Thinh, N.T., 2021. Using a cable-driven parallel robot with applications in 3D concrete printing. Appl. Sci. 11 (2), 563.

Tickoo, S., 2018. CATIA V5-6R2018 for designers. Cadcim Technologies.

Valizadeh, M., Wolff, S.J., 2022. Convolutional neural network applications in additive manufacturing: A review. In: Advances in Industrial and Manufacturing Engineering. 100072.

Wangler, T., Lloret, E., Reiter, L., Hack, N., Gramazio, F., Kohler, M., Bernhard, M., Dillenburger, B., Buchli, J., Roussel, N., et al., 2016. Digital concrete: opportunities and challenges. RILEM Tech. Lett. 1, 67–75.

Wolfs, R.J., Salet, T.A., Roussel, N., 2021. Filament geometry control in extrusion-based additive manufacturing of concrete: The good, the bad and the ugly. Cem. Concr. Res. 150, 106615.

Wu, P., Ramani, K.S., Okwudire, C.E., 2021. Accurate linear and nonlinear model-based feedforward deposition control for material extrusion additive manufacturing. Addit. Manuf. 48, 102389.

Yan, J., Demirci, E., Ganesan, A., Gleadall, A., 2022. Extrusion width critically affects fibre orientation in short fibre reinforced material extrusion additive manufacturing. Addit. Manuf. 49, 102496.

Yuan, P.F., Zhan, Q., Wu, H., Beh, H.S., Zhang, L., 2022. Real-time toolpath planning and extrusion control (rtpec) method for variable-width 3D concrete printing. J. Build. Eng. 46, 103716.

Zhang, Z., 2000. A flexible new technique for camera calibration. IEEE Trans. Pattern Anal. Mach. Intell. 22 (11), 1330–1334.

Zhang, X., Liou, F., 2021. Introduction to additive manufacturing. In: Additive Manufacturing. Elsevier, pp. 1–31.

Zhang, Y., Zhang, Y., Yang, L., Liu, G., Chen, Y., Yu, S., Du, H., 2021. Hardened properties and durability of large-scale 3D printed cement-based materials. Mater. Struct. 54 (1), 1–14.

Zhao, X., Landers, R.G., Leu, M.C., 2010. Adaptive extrusion force control of freeze-form extrusion fabrication processes. J. Manuf. Sci. Eng. 132 (6).

Zomorodi, H., Landers, R.G., 2016. Extrusion based additive manufacturing using explicit model predictive control. In: 2016 American Control Conference. ACC, IEEE, pp. 1747–1752.